Journal of Hydrology (2006) 331, 103–109

available at www.sciencedirect.com

ScienceDirect

journal homepage: www.elsevier.com/locate/jhydrol

The influence of ambient groundwater discharge on exchange zones induced by current–bedform interactions

M. Bayani Cardenas *, J.L. Wilson

Department of Earth and Environmental Science, New Mexico Institute of Mining and Technology, MSEC 208, 801 Leroy Place, Socorro, NM 87801, United States

Received 15 December 2005; received in revised form 3 May 2006; accepted 5 May 2006

KEYWORDS
Coupled flow modeling;
Stream–aquifer interaction;
Sediment–water interface;
Bedform;
Hyporheic exchange zone;
Submarine groundwater discharge;
FEMLAB

Summary We use numerical modeling to investigate the interactions between laminar flow in a water column, current–bedform induced flow in underlying permeable sediments, and discharge of deep groundwater to the water column. Groundwater discharge reduces the spatial extent of current-induced exchange zones within the sediments and may completely prevent the development of current–bedform induced flow at high groundwater discharge. Although exchange zone size is reduced by groundwater discharge, the reduction in exchange flux is not significant, suggesting reduced residence times of materials cycled through these smaller zones. Fluid exchange zones tend to be centered around the reattachment points of eddies that also mark the location of flow divides within the sediments; while deep groundwater is discharged preferentially along troughs. Exchange zone depth and the water column Reynolds number are functionally related through a Morgan–Mercer–Flodin model. The relationship between the current-induced flux through the sediments and the Reynolds number is described by low-order monotonic polynomial functions.

Introduction

The biogeochemical processes occurring along sediment–water interfaces (SWIs) have measurable impacts on the distribution of ecologically and environmentally important substances up to the watershed scale in the case of rivers (Harvey and Fuller, 1998) and lakes, and up to the global scale in the case of estuaries (Webster et al., 1996) and oceans (Riedl et al., 1972). Transport of biogeochemically important solutes along and across these interfaces can either be diffusive or advective. Fluid flow through the permeable sediments is generated by several mechanisms including wave and tidal pumping (Riedl et al., 1972, 1993), flushing due to flow over irregular surfaces such as bedforms and obstacles (Thibodeaux and Boyle, 1987, 1992, 2003), and biogenic processes. In this paper, we only

* Corresponding author. Tel.: +1 505 835 5484; fax: +1 505 835 6436.
E-mail address: cardenas@nmt.edu (M. Bayani Cardenas).

0022-1694/$ - see front matter © 2006 Elsevier B.V. All rights reserved.
doi:10.1016/j.jhydrol.2006.05.012

consider flushing due to current–bedform interactions. When the sediments are sufficiently permeable advective transport becomes more important than diffusion. Thus, in permeable sediments, biogeochemical processes are strongly governed by or coupled to hydrodynamical processes (Huettel et al., 2003). Unfortunately, much remains to be understood regarding the fluid physics along and across SWIs. Discharging groundwater influences and further complicates the physics and biogeochemistry of both porewater and benthic–water (Burnett et al., 2003). However, groundwater discharges into most continental and intra-island surface water bodies (Winter et al., 1998), and it is widely accepted that groundwater from coastal confined and unconfined aquifers can be discharged along beaches and even deeper parts of the continental shelf up to as much as 80 km away from the coast (Moore, 1996, 1998, 2003). Our already restricted understanding of coupled fluid flow in the water column and underlying sediments is further limited for systems with ambient groundwater discharge (AGD). To our knowledge, the impact of AGD on the hydrodynamics of SWIs has not been investigated either in experimental (field and laboratory) or theoretical studies, although Woessner (2000) presented some conceptual models. Our aim is to examine the fluid dynamics along SWIs where there is discharging groundwater.

Methodology

We address this goal through numerically modeling the steady-state two-dimensional flow along SWIs. We assume laminar flow in the water column and porous media Darcy flow in the underlying sediments. The modeling is implemented in FEMLAB, a multiphysics finite element analysis software. The code solves the Navier–Stokes (NS) and continuity equations for incompressible, viscous flow for the water column:

$$\rho\frac{\partial \mathbf{u}}{\partial t} - \mu\nabla^2\mathbf{u} + \rho(\mathbf{u}\cdot\nabla)\mathbf{u} + \nabla p = 0 \quad (1)$$

$$\nabla\cdot\mathbf{u} = 0 \quad (2)$$

where ρ is fluid density, $\mathbf{u}$ is the velocity vector, μ is dynamic viscosity, and p is pressure.

The porous bed domain is governed by the combination of Darcy's Law and the continuity equation for incompressible flow in a non-deformable media, i.e., the groundwater flow equation:

$$\nabla\cdot\mathbf{q} = 0 \quad (3)$$

$$\mathbf{q} = -\frac{k}{\mu}\nabla p \quad (4)$$

where $\mathbf{q}$ is the specific discharge (i.e. Darcy ''velocity'') and k is intrinsic permeability. Direct solvers from the UMFPACK algorithm (Davis, 2004) are implemented in FEMLAB. Sequential coupling is implemented via imposing the NS-continuity derived pressure distribution from the bottom of the water column as a Dirichlet boundary at the top of the bed surface, for the groundwater flow equation.

The top of the water column is treated as a no-flow symmetry boundary and not as a free surface (Fig. 1), while its bottom boundary, the sediment–water interface (SWI), assumes the no-slip/no-flow condition. Because the top boundary of the porous domain is a prescribed pressure boundary, derived from solving the NS equations in the water column, the pressure is continuous across the two domains. The lower boundary of the porous domain is a prescribed-flux boundary, thereby representing ambient groundwater discharge upward to the water column. Periodic boundaries are used on the left and right (Fig. 1) of both domains. Fluid properties are those of fresh water at standard and isothermal conditions (20 °C). The sediment is assigned a permeability (k) of 10^{-10} m^2. Examples of simulated flow fields are shown in Fig. 2.

Multiple simulations with varying parameters were conducted. We varied the bedform length (L), and therefore the height/length ratios or steepness (H/L), in the range of observed fluvial dune geometries, and the prescribed ambient groundwater flux density at the base, q_{bas}, which we refer to as ''basal flux''. The average velocity in the water column, U_{ave}, was varied via changing prescribed pressure gradients between the two periodic side boundaries. Flow is typically turbulent in rivers, estuaries, and oceans, but we only model laminar conditions in the water column, across the entire range of U_{ave} values.

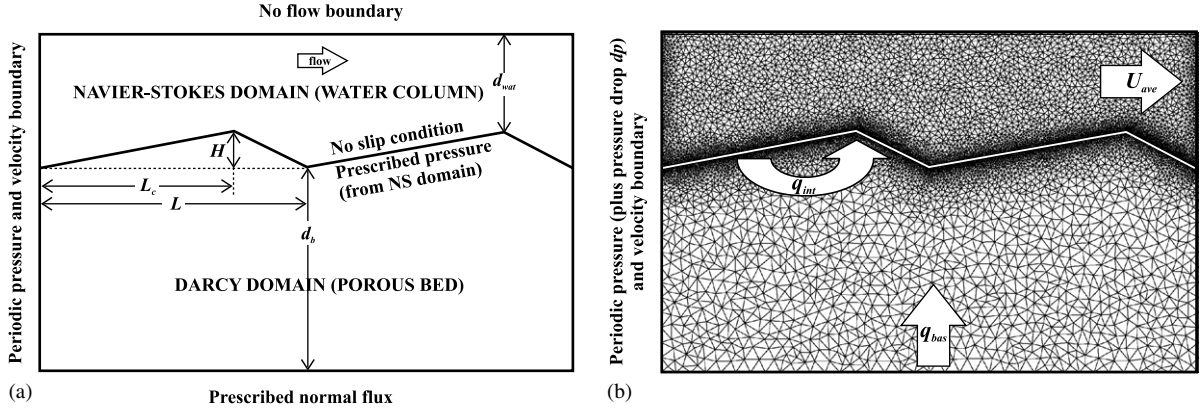

Figure 1 (a) Schematic of model domain and system formulation. (b) Representative finite element mesh illustrating exchange flux through the bed surface, q_{int}, prescribed basal flux, q_{bas}, and average horizontal velocity in the water column, U_{ave}. In all simulations $L_c/L = 0.9$, $H = 0.05$ m and $d_{wat} = 0.45$ m.

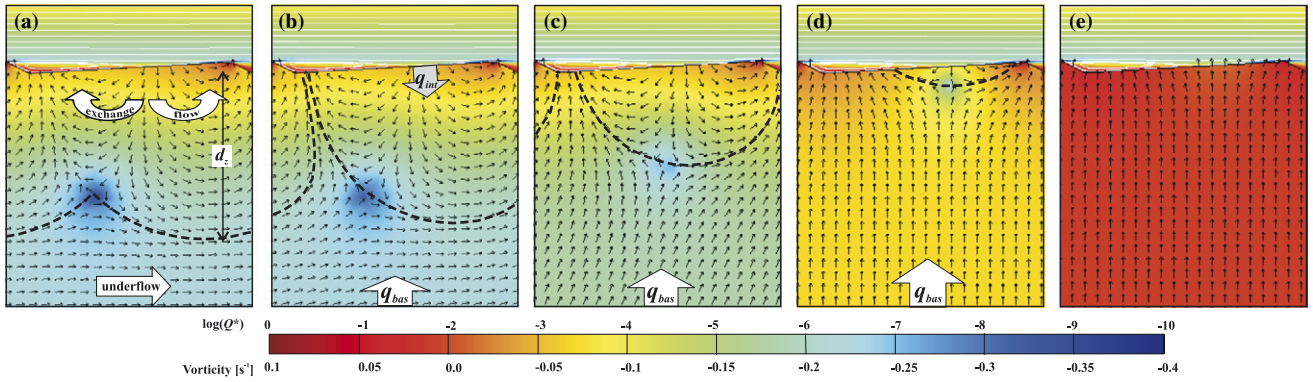

Figure 2 Plots of water column flow streamlines (white lines) and vorticity (color contours), porous bed velocity magnitude (color contours, $Q^* = Q/Q_{max}$, where Q and Q_{max} are the velocity magnitude and the maximum based on all simulations, respectively) and direction (small black arrows), and exchange zone boundaries for different dimensionless ambient basal fluxes, $q^*_{bas} = 0$, 1.8e − 6, 5.5e − 6, 1.8e − 5 and 1.8e − 4 for a–e, respectively. The dashed black line is a dividing streamline which separates the interfacial exchange zone from deeper zones dominated by ambient underflow or upwelling groundwater flow; the vertical distance (see (a)) from the trough to the deepest section of this streamline defines the depth of the exchange zone, d_z. Also illustrated are the normal flux through the SWI (large gray arrow in b) induced by current–bedform interactions, q_{int}. Re = 1500 for all simulations. H = 0.05 m, L = 1.0 m, and d_b = 2 m.

Results and discussion

We refer to the volume within the permeable sediments that is physically influenced by fluid exchange across the SWI as the interfacial exchange zone (IEZ). The IEZ is analogous to the ''hyporheic zone'' in fluvial settings. The maximum depth of the IEZ, d_z, is taken as the distance between the deepest portion of the streamline which envelopes all streamlines originating from the SWI, and the trough of the bedform (Fig. 2a). The IEZ flux density through the SWI is computed as follows: (i) first, total volumetric flux through the SWI per bedform is computed by integration of the magnitude of the normal flux along the bedform surface; (ii) then, we subtract from this total volumetric flux the prescribed volumetric basal flux (basal flux multiplied by the bedform length) resulting in the total volumetric interfacial flux that is induced solely by current–bedform interactions; (iii) the resulting quantity is divided by the twice the length of the bedform because the integration does not discriminate between induced flux going in and out of the bed, which are approximately equal. The final value, q_{int}, is an effective flux density based on bedform length; the total IEZ flux is given by the product $q_{int}L$ and takes place only for that portion of the SWI subjected to current-induced flushing (bounded by the dividing streamline discussed above and shown in Fig. 2). The basal and interfacial flux densities, which are schematically represented in Fig. 1b, are nondimensionalized as follows:

$$q^* = q/K \tag{5}$$

where q^* is the dimensionless flux density and $K = k\rho g/\mu$ is the hydraulic conductivity of the sediments.

Eddies and pore-water flow divides

The simulated flow fields illustrate the relationship between flow conditions above and below the SWI (Fig. 2). We implement sequential and not simultaneous coupling which prevents any feedback effects of discharging groundwater to the water column flow field. The water column dynamics therefore follows the same behavior that is described in detail by Cardenas and Wilson (submitted for publication). Note in particular the eddy downstream of the bedform. The pore-water circulating through the IEZ can be divided into two cells, one discharging towards the crest and the other towards the trough. The dividing streamline separating the two cells starts at the eddy reattachment point on the SWI. As the dimensionless basal flux q^*_{bas} increases, the volume of the IEZ diminishes but remains more or less centered around the eddy reattachment point. The Darcy velocity magnitude within the IEZ also decreases. This decrease is small when q^*_{bas} is also small (compare Fig. 2a with Fig. 2c for example). Thus, although the spatial extent of the IEZ is diminished significantly by discharging groundwater, the amount of material cycled through these smaller zones stays about the same as for the case with no AGD (more on this later). The preferential discharging of ambient groundwater along the troughs may have biogeochemical consequences. We therefore expect the discharge areas close to the troughs, where two different waters mix, to be a biogeochemical or ecological ''hotspot''. When groundwater discharge becomes large enough, the flow field within the sediments is eventually reduced to an upward (more or less) uniform flow field typical of homogeneous porous media subjected to a uniform flux or pressure gradient (Fig. 2e).

Effect of Reynolds number

We examined how the water column Reynolds number (Re) affects exchange zone depth, d_z, and dimensionless interfacial flux, q^*_{int}. Re is defined as follows:

$$Re = \frac{U_{ave}H}{\nu} \tag{6}$$

where U_{ave} is the average velocity along a vertical-section in the water column taken from the crest of the bedform to

the top boundary, H, the height of the bedform, is the characteristic length scale and ν is kinematic viscosity of water. The impact of varying Re was analyzed for different bedform steepnesses or aspect ratios (H/L; H = 0.05 m for all cases), but when plotted dimensionlessly the results are the same (Fig. 3a); the data corresponding to different steepnesses falls on one curve when d_z is normalized by L. A universal threshold Re between laminar–transitional–turbulent flow regimes for triangular bedforms is not well-documented. Defining a threshold becomes more difficult when multiple geometries are considered, such as our case. In this paper we present results at higher Re's where actual flow may no longer be laminar for these reasons as well as for completeness. Additionally, presenting results through the transitional regime facilitates comparison with similar future multiphysics studies that explicitly consider transitional and/or turbulent flows in the water column.

For a given groundwater discharge rate, the d_z increases with Re, sharply at low Re as the eddy grows, and then starts to become asymptotic at higher Re (Fig. 3a) as the eddy reaches it maximum size. When q^*_{bas} is present, the sharp growth in d_z/L is subdued (Fig. 3a), and there is a threshold or critical Reynolds number, Re_{crit}, below which there is no IEZ, and the sediments are completely filled with discharging basal groundwater (Fig. 2e).

In the absence of AGD, the relationship between Re and d_z (or d_z/L) can be described (Cardenas and Wilson, submitted for publication) by a Michaelis–Menten (MM) functional model (Michaelis and Menten, 1913). This function passes through the origin when there is no basal flux. However, Fig. 3a shows that when AGD is present, the MM model is no longer appropriate because of the threshold effects and a more general form is warranted. We therefore fit the Morgan–Mercer–Flodin (MMF) model (Morgan et al., 1975) to the simulation results in Fig. 3a and for four other basal flux scenarios (Fig. 3b and Table 1). The MMF model was originally developed to describe the nutritional response of higher organisms and is defined as

$$(d_z/L) = \frac{(ab + cRe^d)}{(b + Re^d)} \tag{7}$$

The x-intercept of the fitted MMF models represents the critical Reynolds number. The limit of d_z/L, the coefficient c, approaches 1 when there is no AGD (Cardenas and Wilson, submitted for publication). Fig. 3b, which depicts fitted MMF curves (R > 0.99 for all cases), shows that the maximum d_z/L is less than 1 when q_{bas} > 0 and decreases with increasing q^*_{bas}, illustrating the expected competing roles of AGD and current–bedform interactions. Fig. 3b also illustrates how Re_{crit} increases with q^*_{bas}. The relationship between Re_{crit} and q^*_{bas} is also described by a MMF model (Fig. 4 and Table 2). As the magnitude of AGD increases (increasing q^*_{bas}), the current in the water column needs to generate larger pressure gradients along the bedform surface if it is to force water into the sediments to form an IEZ.

Unlike d_z which follows a saturation growth curve-type model, the IEZ flux induced by water-column flow continually increases with Re (Fig. 3c). Recall that the total IEZ flux

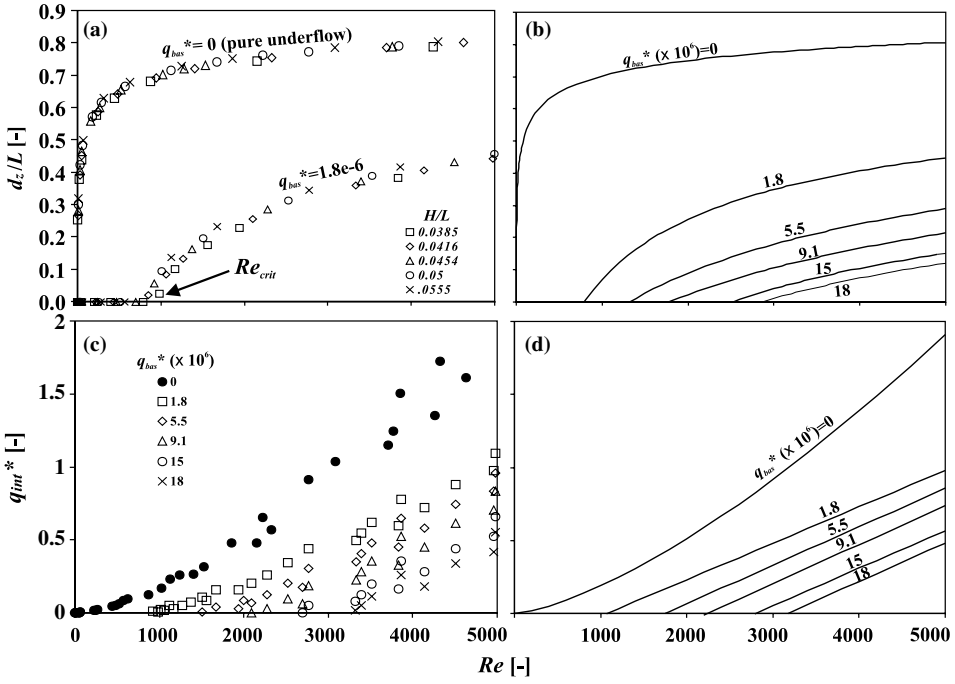

Figure 3 Dependence on Re of normalized exchange zone depth d_z/L (a, b) and dimensionless interfacial flux q^*_{int} (c, d). Shown are results for different bedform aspect ratios (H/L; H = 0.05 m for all cases) and dimensionless basal fluxes q^*_{bas}. The curves in (b) and (d) are fitted for different q^*_{bas} (see Table 1 for fitting parameters); MMF fits are shown in (b) and linear fits are shown in (d). Flow in the water column may be transitional or turbulent at higher Res. No additional considerations were made to correct for turbulent flow. Thus, the simulation results at high Res may be inconsistent with real scenarios but are still presented because thresholds for the different bedform shapes are not yet well established. d_b varies from 2 m to 2.5 m where cases with larger L correspond to larger d_b.

Table 1 Fitting parameters corresponding to the curves in Fig. 3

q_{bas} ($\times 10^6$)	1.8	5.5	9.1	15	18
MMF fits (Eq. 7) in Fig. 3b: $d_z/L(Re)$					
a	−1.18	−0.3	−0.51	−1.04	−0.85
b	46.3	91.2	138.1	81.9	107.6
c	0.78	0.91	1.04	0.58	0.62
d	0.64	0.58	0.57	0.64	0.64
R^2	0.988	0.977	0.929	0.910	0.856
Linear fits in Fig. 3d: $q^*_{int} \times 10^6(Re)$					
a (−)	0.268	0.459	0.603	0.718	0.841
b ($\times 10^4$)	2.50	2.63	2.69	2.57	2.65
R^2	0.981	0.965	0.949	0.907	0.911
Quadratic fits based on Fig. 3c: $q^*_{int} \times 10^6(Re)$					
a (−)	0.145	0.210	0.249	−0.04	0.650
b ($\times 10^4$)	1.347	0.901	0.554	−0.15	1.708
c ($\times 10^8$)	2.049	2.668	3.00	5.245	1.131
R^2	0.988	0.974	0.958	0.921	0.911

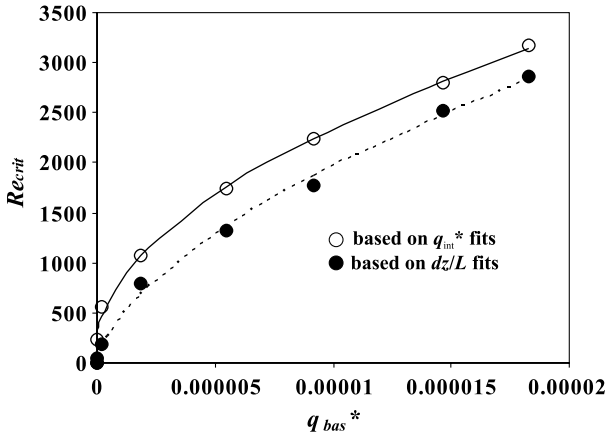

Figure 4 Relationship between Re_{crit} and q^*_{bas} including fitted MMF models (see Table 2).

Table 2 Fitted MMF models to Fig. 4

Data	R^2	a	b	c	d
d_z/L	0.998	20.2	0.02	62,553	0.638
q^*_{int}	0.999	218.6	−136	−1.3e − 8	0.531

is given by the product LKq^*_{int}. The relationship between Re and q^*_{int} simulation results can be fit with either a quadratic or a linear model (Table 1). Fig. 3d shows fitted linear models for the cases where basal flux, q^*_{bas}, is non-zero. As q^*_{bas} approaches 0, a quadratic model is more appropriate, as shown for the case where $q^*_{bas} = 0$ (top line in Fig. 3d). A second estimate of a critical Reynolds number can be defined based on the q^*_{int} information (Fig. 3d and Table 2). The values for Re_{crit} based on liner regression of the q^*_{int} (Re) values is systematically higher than those based on MMF regression of the d_z/L (Re) values (partly due to the linear fit missing the curvature at lower Re values). However, the MMF-behavior of Re_{crit} (q^*_{bas}) is alike for both cases (Fig. 4).

Residence times through the exchange zones

The characteristic (mean) residence time through a system can be estimated by dividing the volume of the domain through which the fluid is flowing, by the steady volumetric flux, and multiplying by porosity, n. In our case, the total flux through the IEZ is represented by the product LKq^*_{int}. In our two-dimensional model the volume of the IEZ becomes an area, A, defined by dashed lines in Fig. 2 and the sediment–water interface. The mean residence time is then estimated as nA/LKq^*_{int}. Defining a dimensionless area, $A^* = A/A_{max}$, where A_{max} is the maximum IEZ area which corresponds to the area of the IEZ when $q_{bas} = 0$ (e.g., Fig. 2a), the dimensionless mean residence time is defined as

$$t^* = \frac{A^*}{q^*_{int}} \tag{8}$$

Some t^* values are presented in Fig. 5a. The characteristic residence times decrease with increasing basal flux with a smaller rate of decrease at larger basal fluxes. This behavior is consistent with the qualitative aspects of the flow field shown in Fig. 2, and quantitative measures in Fig. 5b. The velocities near the interface (Figs. 2a–c) and the interfacial fluxes (Fig. 5b) decrease only slightly, while the IEZ area decreases much more. The amount of fluid pumped through the IEZ$(= LKq^*_{int})$ stays about the same over the range of AGD, despite the smaller size of the IEZ.

Summary

We investigated the flow dynamics along and across an irregular sediment–water interface subjected to ambient groundwater discharge (AGD) via sequentially-coupled numerical flow modeling. The governing equations are the Navier–Stokes equations for laminar flow in the water

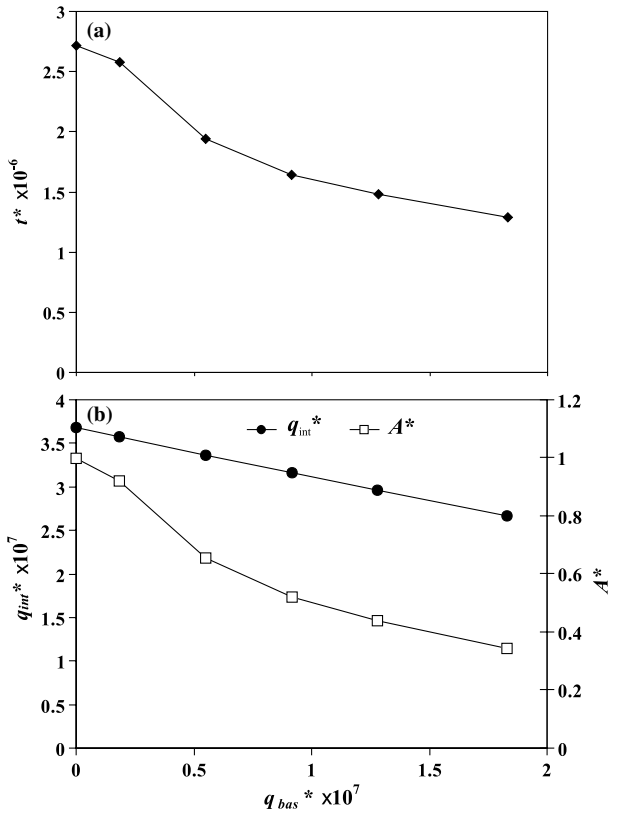

Figure 5 Relationship of t^*, q^*_{int} and A^* with q^*_{bas}. Re = 500 for all simulations; H = 0.05 m, and L = 1 m.

column and the groundwater flow equation for the porous bed; they are solved using the multi-physics finite-element software FEMLAB. To our knowledge, coupled systems with AGD have not been studied in detail theoretically, experimentally, or in natural settings.

Numerical experiments were designed to investigate the competing roles of flow through the sediment–water interface induced by current–bedform topography interactions and by AGD, and to see how the bedform geometry and the conditions in the water column affect the size of and fluxes through the interfacial exchange zone (IEZ) in the porous bed. Water column eddy reattachment points coincide with flow divides within the bed. The cases with no AGD are studied in detail in Cardenas and Wilson (submitted for publication). As the AGD increases, the IEZ gets significantly smaller yet remains approximately centered around the eddy reattachment points. The AGD tends to focus near the bedform troughs suggesting that there might be localized biogeochemical hotspots where the two waters mix.

We found that the IEZ develops only when a current threshold is overcome. This threshold is quantified by a critical Reynolds number, below which groundwater discharging to the water column overpowers any interfacial exchange driven by current–bedform interactions. Above this current threshold, the IEZ deepens sharply with further increase in the Reynolds number and then stabilizes at an asymptotic depth that is less than the length of the bedform. The sharp deepening of the IEZ becomes more gradual, and the asymptotic IEZ depth smaller, with an increase in AGD.

When AGD is absent, the functional relationship between the Reynolds number and the IEZ depth is described by the Michaelis–Menten type model. However, it is modified to the more general Morgan–Mercer–Flodin model, whose x-intercept is no longer at the origin, when the system is influenced by AGD. The x-intercept (representing the critical or threshold Reynolds number) increases with and is related to the ambient groundwater flux also via a Morgan–Mercer–Flodin functional model.

The non-asymptotic relationship between interfacial flux, induced by current–bedform interactions, and Reynolds number is described by quadratic or linear regression models. An increase in AGD results in relatively small changes in induced interfacial flux, especially when compared to the reductions in the IEZ spatial extent. Thus, AGD, while reducing the extent of IEZs, does not substantially impact the amount of fluid and materials transported through these zones (except when the zones are of very limited extent or non-existent), suggesting reduced residence times.

Our results have implications for the biogeochemistry of sediment–water interfaces where material transport is primarily advective. However, because our approach assumes laminar flow conditions in the water column, the results should be taken as explanatory of the hydrodynamic processes rather than predictive, for most natural flows are turbulent.

Acknowledgements

MBC was supported by the Kottlowski Fellowship of the New Mexico Bureau of Geology and Mineral Resources at the New Mexico Institute of Mining and Technology (NMIMT). Computing resources were provided by the Department of Earth and Environmental Sciences at NMIMT. We acknowledge the technical support by Comsol, Inc.

References

Burnett, W.C., Bokuniewicz, H., Huettel, M., Moore, W.S., Taniguchi, M., 2003. Groundwater and pore water inputs to the coastal zone. Biogeochemistry 66, 3–33.

Cardenas, M.B., Wilson J.L., submitted for publication. Hydrodynamics of coupled flow above and below a sediment–water interface with triangular bedforms. Advances in Water Resources

Davis, T.A., 2004. A column pre-ordering strategy for the unsymmetric-pattern multifrontal method. Association for Computing Machinery Transactions on Mathematical Software 30 (2), 165–195.

Harvey, J.W., Fuller, C.W., 1998. Effect of enhanced manganese oxidation in the hyporheic zone on basin-scale geochemical mass balance. Water Resources Research 34 (4), 623–636.

Huettel, M., Gust, G., 1992. Impact of bioroughness on interfacial solute exchange in permeable sediments. Marine Ecology Progress Series 89, 253–267.

Huettel, M., Roy, H., Precht, E., Ehrenhauss, S., 2003. Hydrodynamical impact of biogeochemical processes in aquatic sediments. Hydrobiologia 494, 231–236.

Michaelis, L., Menten, M.L., 1913. Die kinetik der invertinwirkung (The kinetics of invertase activity). Biochemische Zeitschrift 49, 333–369.

Moore, W.S., 1996. Large groundwater inputs to coastal waters revealed by ^{226}Ra enrichments. Nature 380, 612—614.

Moore, W.S., Shaw, T.J., 1998. Chemical signals from submarine fluid advection onto the continental shelf. Journal of Geophysical Research 103 (C10), 543—552.

Morgan, P.H., Mercer, L.P., Flodin, N.W., 1975. General model for nutritional responses of higher order mechanisms. Proceedings of the National Academy of Sciences of the United States of America 72 (11), 4327—4331.

Riedl, R.J., Huang, N., Machan, R., 1972. The subtidal pump: A mechanism of interstitial water exchange by wave action. Marine Biology 3, 210—221.

Shum, K.T., 1993. The effects of wave-induced pore water circulation on the transport of reactive solutes below a rippled water-sediment interface. Journal of Geophysical Research 98C, 10289—10301.

Thibodeaux, L.J., Boyle, J.D., 1987. Bedform-generated convective-transport in bottom sediments. Nature 325, 341—343.

Webster, I.T., Norquay, S.J., Ross, F.C., Wooding, R.A., 1996. Solute exchange by convection within estuarine sediments. Estuarine Coastal and Shelf Science 42, 171—183.

Winter, T.C., Harvey, J.W., Franke, O.L., Alley, W.M., 1998. Ground Water and Surface Water: A Single ResourceUnited States Geological Survey Circular, 1139. USGS, Denver.

Woessner, W.W., 2000. Stream and fluvial plain ground water interactions: rescaling hydrogeologic thought. Ground Water 38, 423—429.